Heliyon 7 (2021) e07023

Contents lists available at ScienceDirect

Heliyon

journal homepage: www.cell.com/heliyon

Research article

Investigation of the effects of electrochemical reactions on complex metal tribocorrosion within the human body

Thomas S. Welles *, Jeongmin Ahn

Department of Mechanical and Aerospace Engineering, Syracuse University, Syracuse, NY 13244-1240, USA

ARTICLE INFO

Keywords:
Total hip arthroplasty
Tribocorrosion
Oscillatory electrochemical corrosion
Electric potential oscillation
Implant failure
Non-mechanically driven wear
Fretting
Crevice corrosion

ABSTRACT

Although total hip arthroplasty (THA) is considered to be the most successful orthopedic operation in restoring mobility and relieving pain, common Metal-on-Metal (MoM) implants developed in the past decade suffer from severe inflammatory reactions of the surrounding tissue caused by the premature corrosion and degradation of the implant. A substantial amount of research has been dedicated to the investigation of mechanically driven fretting and crevice corrosion as the primary mechanism of implant failure. However, the exact mechanism by which hip implant breakdown occurs remains unknown, as current *in vitro* fretting and crevice corrosion studies have failed to completely replicate the corrosion characteristics of recovered implants. Here, we show that minor electric potential oscillations on a model hip implant replicate the corrosion of failed implants without the introduction of mechanical wear. We found in a controlled lab setting that small electrical oscillations, of similar frequency and magnitude as those resulting from ambient electromagnetic waves interacting with the metal of the implant, can force electrochemical reactions within a simulated synovial fluid environment that have not been previously predicted. In lab testing we have shown the replication of titanium, phosphorous, and oxygen deposition onto the surface of ASTM astm:F75 CoCrMo metal alloy test specimens, matching the chemical composition of previously retrieved wear particles from failed patient prosthetics. Our results demonstrate that the electrical activity and ensuing electrochemical activity excites two corrosion failure modes: direct dissolution of the medically implantable alloy, leaching metal ions into the body, and surface deposition growth, forming the precursor of secondary wear particles. We anticipate our findings to be the foundation for the future development and testing of electrochemically resistant implantable material.

Key Points

Question: Is there an initiating electrochemical step to the corrosion of metal based hip implants prior to mechanical wear beyond natural galvanic reaction?

Findings: Lab testing indicates that electric potential oscillations on the surface of a metal subjected to a simulated body environment more accurately replicate the complex corrosion phenomenon found on retrieved hip implants when compared to previously published data. These electrical oscillations could be induced by natural biologic processes or forced by electromagnetic radiation.

Meaning: New testing procedures for implanted biomaterials, which account for electrical activity, may be warranted to prevent ion leach into the patient.

1. Introduction

Total hip arthroplasty (THA) has been considered to be the most successful operation to both relieve pain and restore mobility from osteoarthritis; however, implant corrosion and wear-related complications remain a daily concern for implant longevity and patient health [1]. In the United States alone, there are over 370,000 THA's performed annually and the number continues to grow each year. It is predicted that over 3 million individuals are currently living with a hip implant [1, 2].

The new generation of Metal-on-Metal (MoM) implants, commonly Cobalt–Chromium–Molybdenum (CoCrMo alloy ASTM astm:F75), developed in the past decade were designed in order to prevent hip dislocation and polyethylene wear complications [2, 3]. It is reported that more than 1 million MoM hip implants have been made worldwide [2]. This generation of hip implants, however, suffers from the

* Corresponding author.
E-mail address: tswelles@syr.edu (T.S. Welles).

https://doi.org/10.1016/j.heliyon.2021.e07023
Received 14 May 2020; Received in revised form 13 July 2020; Accepted 5 May 2021

occurrence of severe inflammatory reactions of the periprosthetic soft tissues. Increased reaction can lead to increased risk of corrosion and wear, resulting in extensive tissue necrosis, injury to abductor muscles and tendons, aseptic loosening/osteolysis, increased revision complications, and significant patient morbidity [4, 5].

Decades of research have been dedicated to discovering the fundamental cause of implant corrosion. It has been found that as the implant wears and corrodes, metal ions are able to leach into the bloodstream resulting in heavy metal toxicity, cognitive dysfunction, mitochondrial stress, organ damage, inflammation, cancer, etc. However, current research does not adequately describe or predict the corrosive chemical breakdown seen in replaced orthopedic implants [6, 7, 8, 9, 10, 11, 12]. Fretting and crevice corrosion are the most common current explanations for implant failure, but these mechanisms focus on a mechanically driven wear while minimizing the potential for a galvanic electrochemical reaction [13, 14, 15, 16, 17, 18, 19, 20]. Additionally, when lab results from simulated fretting corrosion are compared to a failed prosthetic implant, it becomes clear that although fretting may be occurring, it is not a complete explanation. An example of a corroded implant is shown in Figure 1A [21] below. This image is then followed by the industry standard result for fretting and crevice corrosion in Figure 1B [13] (see Figure 2)

Images of Figure 1B clearly replicate the physical wear phenomena seen in the recovered prosthetic in Figure 1A, but does not address the corroded areas. However, if a small electrical oscillation, similar to those experienced by the implant from common electromagnetic radiation sources [22, 23, 24, 25], is applied to the Co and Cr alloy used in medical implant devices, the corrosion begins to replicate that which is seen in recovered prostheses.

2. Method

Samples were cut from medical grade ASTM F75 round stock to serve as a simulated hip implant. The chemical composition of the alloy is found below in Table 1.

The 1" diameter round stock was cross cut, resulting in a 1/8" thick disc. The disc was further sectioned into quadrants. Each quadrant received a 3/32" hole for future wire attachment. The samples were polished to remove any surface imperfections with a Buehler Metaserv 250 Grinder/Polisher and P400 grit silicon carbide wet polishing paper. The curved face of the sample was further polished with P2500 grit silicon carbide wet polishing paper to develop a high sheen, mimicking that of the bearing surface of a hip prosthetic.

Each sample was then wired with a medical grade one titanium wire lead, representative of titanium hardware used in the installation of prosthetic hips. The chemical composition of the titanium wire used is shown in Table 2 below.

Two of the prepared samples were placed into each Pyrex Petri dish, and subsequently submerged in 100 mL of simulated synovial fluid. Each wire lead exited the side of the Petri dish under the lid. The simulated synovial fluid was created following the industry standard of a 1:1 (by volume) mixture of fetal bovine serum (FBS), purchased from Millipore Sigma, and de-ionized (DI) water [13, 14, 15, 16, 17, 18, 19, 20]. The exact chemical composition of the FBS is unknown, but it is known to contain a complex mixture of salts, proteins, and lipids. Any element identified during testing not reported in the metal samples or in the preparation of samples, is assumed to be a result of the FBS.

The samples subjected to electrical activity were connected to a frequency generator for simulated electrical oscillation. A bacteria culture was taken of the simulated synovial fluid and placed within the incubation oven alongside the test specimens in order to identify any contamination within the test fluid. The test specimens were then placed into a faraday cage within an incubation oven at 37 °C for 10 days. For each test, two samples were subjected to electrical oscillations and one baseline sample was shielded from electrical oscillation. Each test run was repeated, resulting in four samples for each test condition to ensure repeatability, as well as two baseline samples. During the duration of the lab testing, the samples subjected to true AC oscillations were connected to an electrochemical impedance spectroscopy (EIS) machine. An EIS response frequency sweep was performed on each specimen daily from

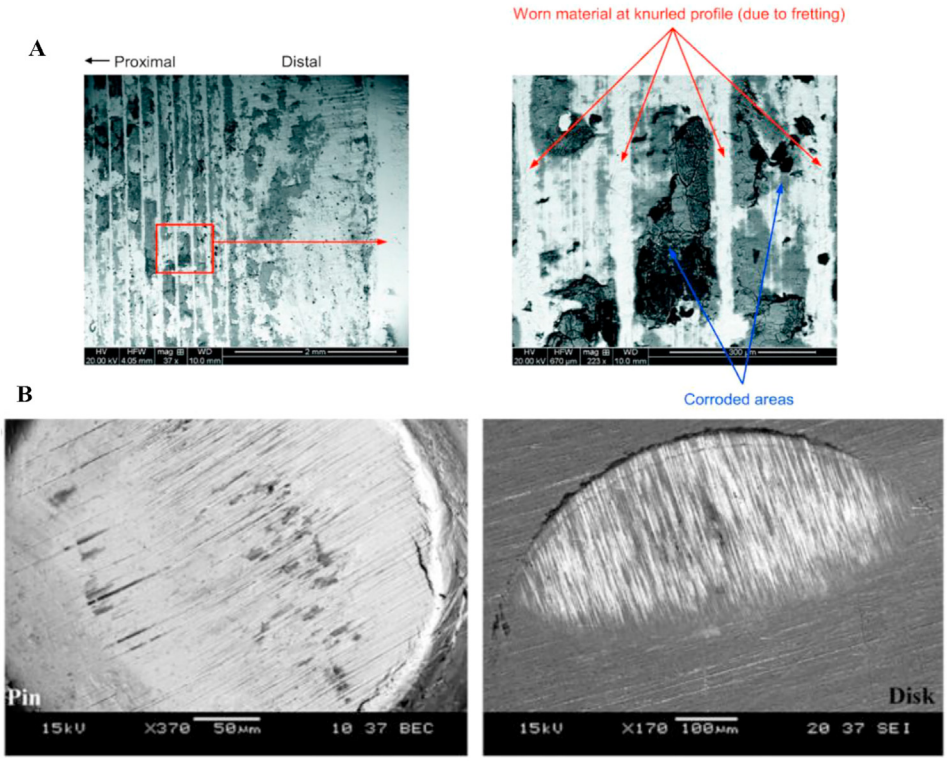

Figure 1. A: Surface damage to the CoCrMo neck, mainly in the distal medial area and scanning electron microscope (SEM) image with a higher magnification showing both mechanical fretting wear and corrosion damage on removed implant. Reprinted from Materials Science and Engineering: C, 79, Oskouei, et al, A new finding on the in-vivo crevice corrosion damage in a CoCrMo hip implant, 390–398, Copyright (2017), with permission from Elsevier [21]. B: Backscatter and secondary electron mode SEM micrographs of pin and disk surfaces of CoCrMo obtained at the end of fretting corrosion in lab testing. Reprinted from Biomaterials, 33, Swaminathan, et al, Fretting corrosion of CoCrMo and Ti6Al4V interfaces, 5487–5503, Copyright (2012), with permission from Elsevier [13].

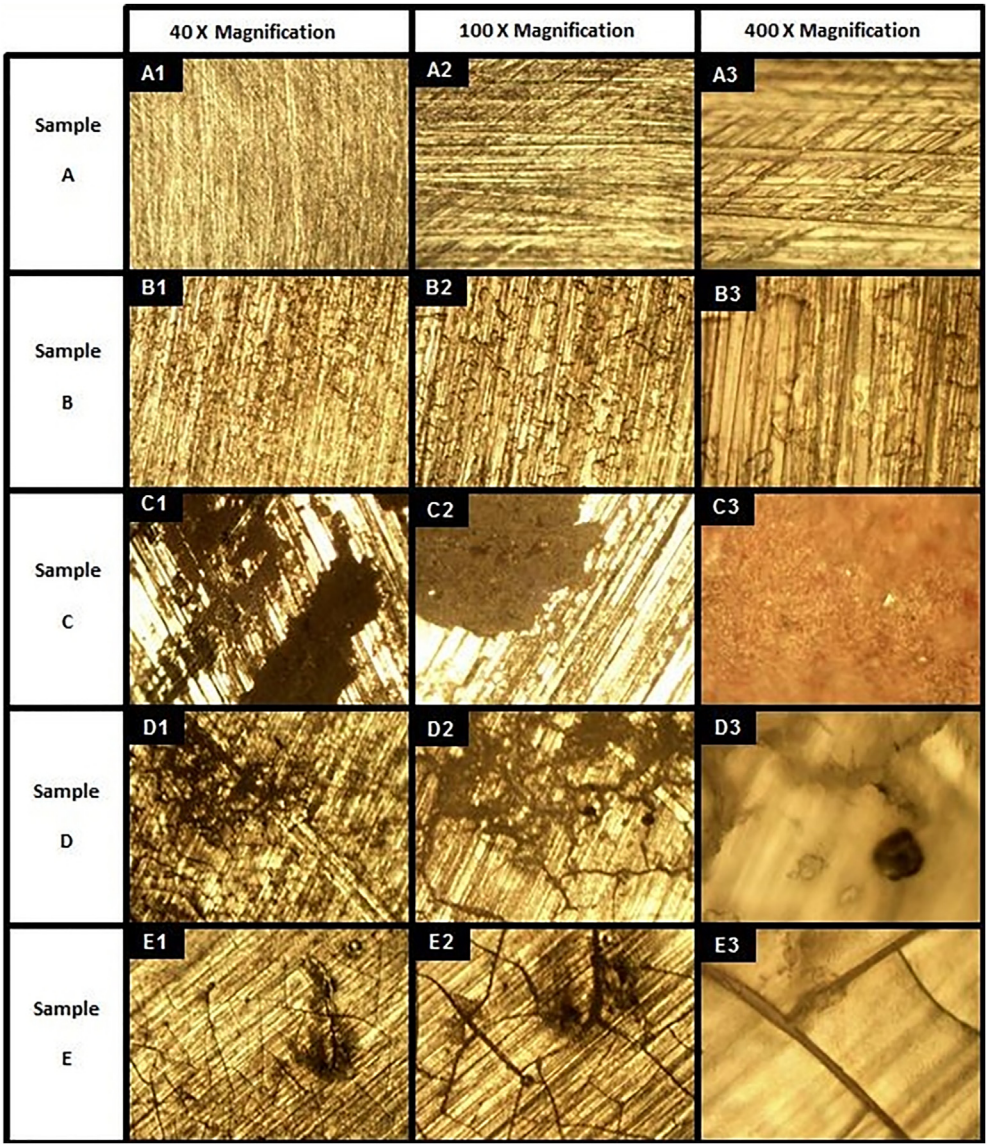

Figure 2. Optical microscopy micrographs of 5 samples under varying electrical test signals. Sample A: Baseline ASTM F75 CoCrMo alloy. Sample B: ASTM F75 CoCrMo alloy placed in simulated synovial fluid (50/50 DI water/FBS) with no electrical signal. Sample C: ASTM F75 CoCrMo alloy in simulated synovial fluid with $V_{rms} = 0.67$ V pulsed DC electrical signal. Sample D: ASTM F75 CoCrMo alloy in simulated synovial fluid with 100 MHz Sine wave at 250 mV peak-to-peak amplitude AC electrical signal. Sample E: ASTM F75 CoCrMo alloy in simulated synovial fluid with 250 mV peak-to-peak amplitude random noise AC electrical signal.

1.5×10^{6} Hz to 5.0×10^{-2} Hz, in order to characterize the electrochemical properties of each specimen. At the conclusion of each test, the samples were removed from the testing solution and rinsed with DI water. The samples were then gently wiped clean with Kimwipes™ to remove any loose material. Following this, the samples were rinsed again with DI water, dried, and bagged for analysis.

Five test conditions were studied to represent a viability study for the first attempt to utilize an oscillatory electrochemical reaction phenomenon to replicate the chemical corrosion of implanted ASTM F75. Samples from test condition A serve as the metal baseline. These samples were not subjected to any testing after sample preparation. Therefore, Sample A represents the clean ASTM F75 sample. Samples from test condition B were placed into simulated synovial fluid with no electrical activity. Samples from test condition C were subjected to a pulsed direct current (DC) signal, consisting of a pulse width modulated signal at a 5 % duty cycle (900 μs pulse on a 20,000 μs period), resulting in a root mean square voltage of 0.67 V. This test condition is meant to investigate an electrophoretic deposition type corrosion mechanism. Skin electrode testing, as well as previously reported literature, has indicated a potential DC offset of skin electrical activity in the range of 500–800 mV [26, 27, 28, 29, 30, 31, 32, 33]. Samples from test condition D were subject to a clean sine wave oscillation at 100 MHz and a peak to peak voltage magnitude of 250 mV. The voltage magnitude was selected in accordance to previously published literature for recorded interference in nerve conduction studies, skin electrode data, and experimental work on biological effects of external electric fields [28, 29, 30, 31, 32, 33, 34, 35, 36, 37, 38]. The corrosion mechanism was additionally assumed to be a high frequency phenomenon, and as such, the frequency of oscillation was set to the generator's upper resolution limit. Samples from test condition E were subjected to a random noise oscillation at a peak to peak amplitude of 250 mV with embedded frequencies up to 100 MHz and no DC offset. This is meant to investigate the effect of noise in comparison to the Sample D test condition.

Samples from test conditions A, B, C, D, and E will be referred to simply as Sample A, etc. and all results shown will be indicative of all samples from that test condition.

3. Results

When electrical activity was placed on the samples within the simulated synovial fluid, samples C-E in Figure 2 began clear corrosion activity. No sample tested here underwent mechanical wear, yet contrary to many theories, corrosion began. The type of surface reaction appears to have a dependency on the frequency of electrical oscillation, indicated by

Table 1. Elemental analysis of CoCrMo metal alloy used in testing provided by United Performance Metals. Testing completed by Carpenter Technology Corporation.

ASTM F75 CoCrMo Alloy Chemical Composition by Weight Percent	
Elements	Weight %
Cobalt	65.05
Chromium	27.76
Molybdenum	5.54
Trace Elements	
Carbon	0.05
Manganese	0.79
Silicon	0.59
Phosphorous	0.003
Sulfur	0.005
Nickel	0.04
Copper	0.01
Aluminum	0.04
Nitrogen	0.175
Titanium	0.004
Tungsten	0.02
Boron	0.001
Iron	0.12

Table 2. Elemental analysis of Titanium Grade 1 wire used in testing provided by TEMCo Industrial.

ASTM F76 Ti Grade 1 Chemical Composition by Weight Percent	
Elements	Weight %
Titanium	≥99.6
Trace Elements	Maximum Weight %
Nitrogen	0.03
Carbon	0.08
Hydrogen	0.01
Iron	0.20
Oxygen	0.18
Maximum Total Residuals	**0.40**

the difference in the appearance of the surface after testing between samples C, D, and E. The combination of samples C-E appear to recreate the corroded areas highlighted by Oskouei et al. in Figure 1A [13]. An application of oscillatory electrical activity, in a magnitude similar to that experienced in daily life, begins to replicate the tribocorrosive behavior seen in failed orthopedic implants.

The surface composition of each sample was then analyzed by energy dispersive X-ray spectroscopy (EDS) Figure 4, the results of which were subsequently compared to published data on the analysis of wear particles retrieved from patient tissue Figure 3.

The samples with electrical activity (Rows C-E) show significant surface modification when compared to the samples without electrical activity (Row B) Figure 4. The surface modification consist primarily of Titanium, Iron, Phosphorous, and Oxygen.

However, the elemental composition differed for each type of electrical oscillation. Sample C was subjected to a pulsed DC signal to identify any effects of DC offset as well as the potential of electrophoretic deposition (EPD). The surface analysis shows removal of Mo and addition of Ti, Fe, and O. The Mo is assumed to have entered solution or is masked by surface deposition. Fe and O are assumed to have deposited from the FBS, whereas the Ti is assumed to have migrated from the wire lead. This surface change is not directly attributed to the potential of EPD because all samples under this test condition showed similar chemical changes. Typically, in EPD, it is expected that charged particles held in colloidal suspension move toward and deposit on the working electrode and move away from the counter electrode. However, in this instance, both electrodes are composed of identical materials and display similar chemical change. It is possible that EPD contributed to the transfer of Ti from the wire lead to the sample surface, yet Sample E also illustrates migration of Ti without the potential for EPD. Therefore, further testing is required to investigate the potential for EPD.

Sample D, under the influence of a clean sine wave oscillation, shows oxygenation of the surface from the FBS, and similar to Sample C, shows loss of Mo.

Sample E, subjected to random noise, shows significant phosphorus presence, unlike any other sample. The phosphorous is assumed to be precipitating onto the surface from the FBS. Although, the ASTM F75 stock used is reported to have 0.003 percent by weight, as shown in Table 1, concentration of phosphorous, all samples were cut from the same stock and no other sample shows significant phosphorous concentration under EDS analysis. Moreover, all samples tested under condition E showed significant presence of phosphorous, whereas all other test condition samples did not show the presence of phosphorous. Sample E, additionally, showed oxygenation of the surface, Ti transfer from the wire lead, and decreased Mo at the surface.

The combination of chemical compositions from the above test conditions begin to replicate that of wear particles reported previously in literature [13, 21, 39]. It is therefore imperative to systematically compare these novel results with previous studies on failed hip implants.

Figure 3 below is taken for comparison from a previous study in which the surrounding tissue of a failed hip implant was sampled to identify wear particles that had released from the surface of the implant. The retrieved particles were analyzed for elemental composition.

As illustrated in Figure 3 [39], the recovered wear particles consisted primarily of Titanium, Iron, Phosphorous, and Oxygen. An inflammatory particle was identified to potentially be Cr_2O_3 [21, 39]. This indicates that the generation of wear particles result from a fundamental chemical change of implanted metal. Current studies of crevice and fretting corrosion do not adequately replicate the significant chemical change seen in implanted devices [13, 21]. The elemental mapping of retrieved wear particles closely matches the results generated by electrical oscillation in Figure 4, above. The experimental work done here was able to demonstrate a precipitation of Titanium, Iron, Phosphorous, and Oxygen as seen in the retrieved particles. The experimental work, however, did not replicate the precipitation of Vanadium. The chemical composition of the patient's synovial fluid is not known, so there is no comparison of Vanadium concentration between the patient and the FBS used in lab testing.

In order to elicit information pertaining to any crystallographic structure change, each sample was further analyzed via X-ray diffraction (XRD). Figure 5, below, illustrates the XRD pattern of each corrosion sample.

Sample A, representing the untested CoCrMo alloy, displays a diffraction pattern with peaks at 2θ equal to 41.3°, 44.1°, 47.1°, 51.0°, and 75.1°. The diffraction pattern is consistent with prior published work [40, 41], identifying the majority of the material as a face centered cubic (FCC) γ-(Co, Cr, Mo) crystallographic structure indicated by peaks at 2θ equal to 44.1°, 51.0°, and 75.1°, as labeled in Figure 5. Lesser peaks at 41.3° and 47.1° indicate a small amount of hexagonal close pack (HCP), ε-(Co, Cr, Mo), as labeled in Figure 5 [41, 42, 43].

The XRD diffraction pattern for Sample B, shielded from electrical activity within simulated synovial fluid, shows no change when compared to Sample A. Therefore, it is concluded that no crystallographic structure change occurred to the metal alloy within the simulated synovial fluid over the test duration.

Sample C, subjected to pulsed DC electrical signal shows significant variation in XRD diffraction pattern when compared to all other samples. Sample C maintains the major FCC) γ-(Co, Cr, Mo) peak at 44.1° from the original alloy, but all other peaks from the original alloy are not present. Sample C shows an additional minor peak at 79.3°, labeled with interplane spacing d = 1.206 Å, and a broad peak between 2θ ~65° and 2θ ~75°, labeled as *, in Figure 5. The lack of the original pattern and

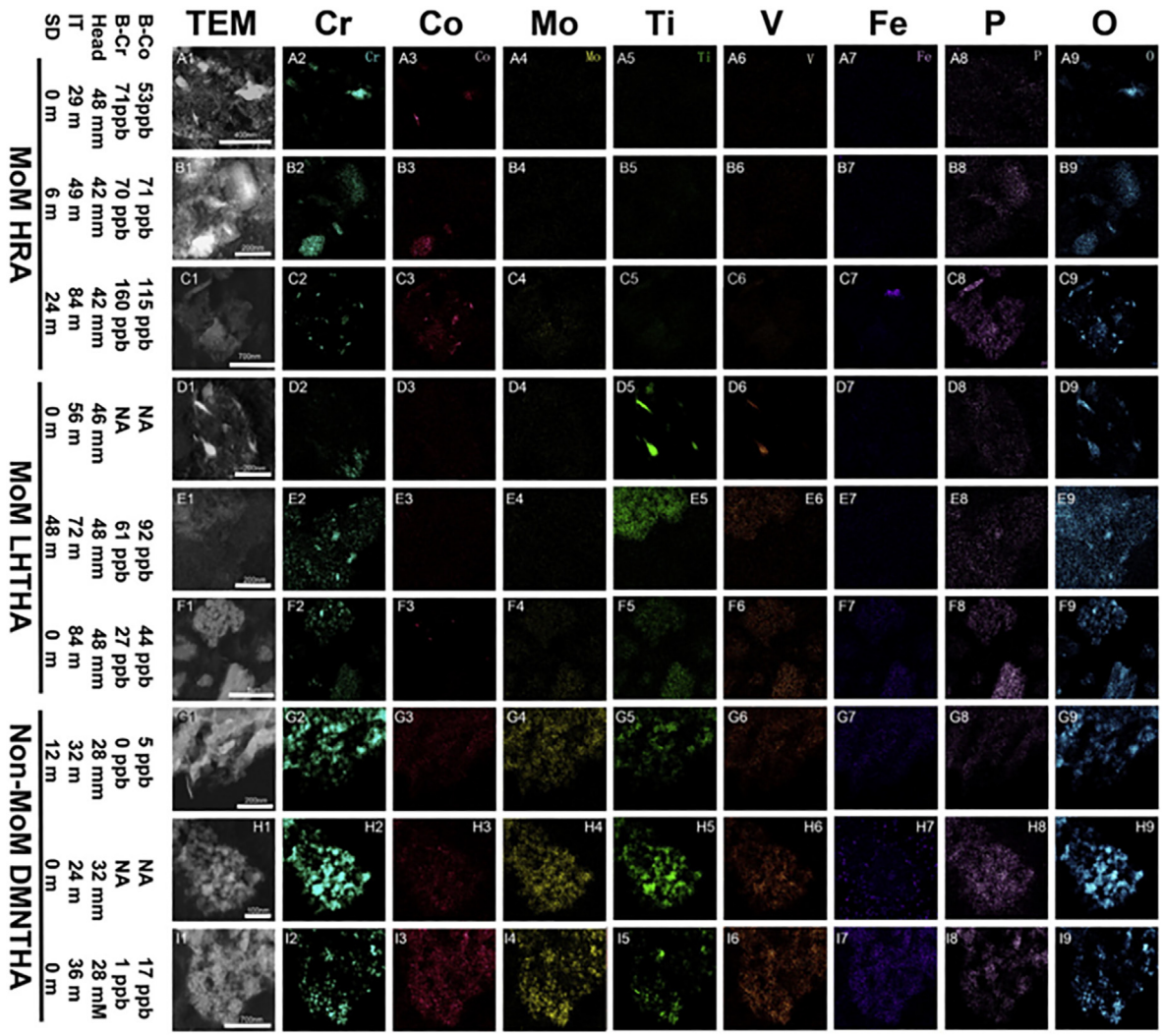

Figure 3. Micrographs of TEM EDS element mapping of three samples of each class of hip arthroplasty. Column A1-I1, TEM micrographs of 9 samples selected for element mapping. All samples contain variable amounts of Cr particles (A2-I2), P (A8-I8) and O (A9-I9). A small number of high electron density particles in the MoM hip resurfacing arthroplasty (HRA) (A3-C3) and the MoM large head total hip arthroplasty (LHTHA) (D3-F3) groups, and the particles in the Non-MoM dual modular neck total hip arthroplasty (DMNTHA) group (G3-I3) contain Co. High concentration of Mo is present in the Non-MoM DMNTHA group (G4-I4) and barely detectable in MoM HRA and MoM LHTHA groups. Ti and Vco-exist in the MoM LHTHA (D5-F5, D6-F6) and the Non-MoM DMNTHA (G5-I5, G6-I6) groups but are not detectable in the MoM HRA group (A5-C5, A6-C6). Fe is detected in some samples (C7, H7 and I7) and does not co-localize with other metal particles. P co-exists with O but its concentration is lower than O.B–Cr, blood Cr ion concentration; B–Co, blood Co ion concentration; Head, femoral head size; IT, implant time; SD, symptom duration. Scale bars: B1, D1, E1, G1 = 200 nm; A1 = 400 nm; C1, I1 = 700 nm; F1 = 1000 nm. Reprinted from Nanomedicine: Nanotechnology, Biology and Medicine, 13, Xia et al, Nano-analysis of wear particles from metal-on-metal and non-metal-on-metal dual modular neck hip arthroplasty, 1205–1217, Copyright (2017), with permission from Elsevier [39].

creation of a broad, non-descript, peak, labeled as * in Figure 5, is believed to be the addition of amorphous material onto the surface of the sample, likely, through EPD and does not indicate structural change within the sample. Previous literature on the analysis of *in-vivo* corrosion products has shown that the original diffraction pattern persists with the potential for additional new peaks [21, 39]. Therefore, on Sample C, EPD is believed to have generated an amorphous deposition masking the original diffraction pattern. The inconstancies between the diffraction pattern of Sample C and previous analysis of corrosion products indicates that EPD is most likely not the cause of corrosion on implanted CoCrMo.

However, if a pure oscillatory electric field is established on samples within simulated synovial fluid, such as with Samples D and E, a clear modification of the original crystallographic structure without the addition of amorphous surface material is evident. Sample D, subjected to a 100 MHz sine wave, and Sample E, subjected to random AC noise, both show the original diffraction pattern of Sample A, peaks at 2θ equal to 41.3°, 44.1°, 47.1°, 51.0°, and 75.1°, with the addition of a substantial peak at 79.3°, with inter-plane spacing d = 1.206Å. Therefore, the majority of the sample is maintained as FCC γ-(Co, Cr, Mo) with a small amount of HCP ε-(Co, Cr, Mo), as labeled in Figure 5. The additional peak at 2θ = 79.3° with inter-plane spacing d = 1.206Å, in conjunction with EDS data given in Figure 4, is believed to be a crystalline product containing Cr, O, and/or P.

This is the first documented tribocorrosive experimental study that has been able to begin to replicate the elemental precipitants on the implant surface without subjecting the metal to mechanical wear. It is hypothesized that the chemical composition of the deposited particulate for the in vitro testing may be tuned in future work via manipulation of the frequency and magnitude of the electrical oscillation to exactly match that of the recovered particles. Therefore, this newly identified electrochemical corrosion mechanism is expected to initiate what has been considered the tribocorrosive decay seen in implanted devices.

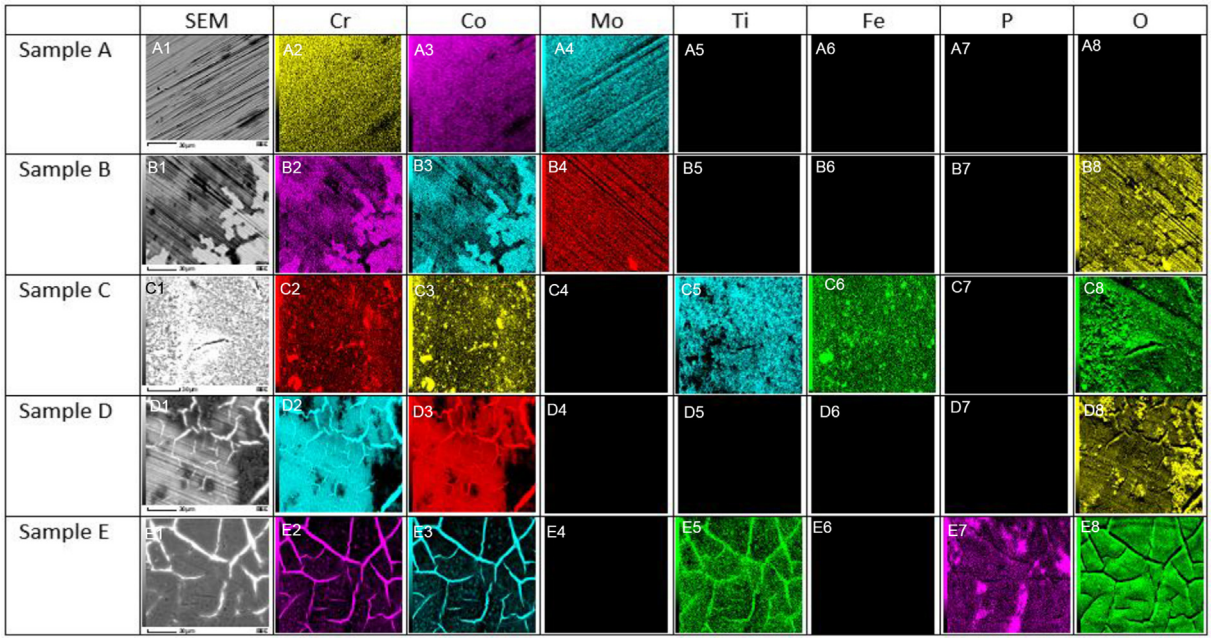

Figure 4. Micrographs of SEM EDS element mapping of 5 samples under varying electrical test signals. Column A1-E1 SEM micrographs of 5 samples selected for elemental mapping after 10 days. Columns 2–8 show detected elements on the sample surface (Chromium-Cr, Cobalt-Co, Molybdenum-Mo, Titanium-Ti, Iron-Fe, Phosphorous-P, and Oxygen-O). Rows A-E identify the sample tested. Sample A: Baseline ASTM F75 CoCrMo alloy. Sample B: ASTM F75 CoCrMo alloy placed in simulated synovial fluid (50/50 DI water/FBS) with no electrical signal. Sample C: ASTM F75 CoCrMo alloy in simulated synovial fluid with $V_{rms} = 0.67$ V pulsed DC electrical signal. Sample D: ASTM F75 CoCrMo Alloy in simulated synovial fluid with 100 MHz Sine wave at 250 mV peak-to-peak amplitude AC electrical signal. Sample E: ASTM F75 CoCrMo alloy in simulated synovial fluid with 250 mV peak-to-peak amplitude random noise AC electrical signal. Note: Colors are randomly assigned by the Jeol SEM, color intensity signifies abundance, and black indicates absence

In order to identify, understand, and potentially predict this electrochemical corrosion mechanism more holistically, the electrochemical behavior change over time is investigated.

The electrochemical behavior of specimens B, D, and E is characterized by the EIS frequency sweep test shown above in Figure 6. Sample C was not characterized by EIS analysis due to machine limitations in conjunction with the pulsed DC signal. The curve labeled 'Baseline Test Start' indicates the electrochemical behavior of all samples prior to testing when first placed into the simulated synovial fluid. The curve labeled as 'Sample B' is the same as in previous figures and is present to act as a control for the experiment. Sample B is allowed to sit within the test fluid, but is not subjected to any forced electrical oscillations, therefore, any changes seen in Sample B may be thought of as baseline changes. As the Sample B concludes testing, there is a clear increase in the imaginary impedance, or reactance of specimen, Figure 6.1, with a minor increase in overall impedance magnitude, Figure 6.2, and phase shift at low frequency (<100 Hz), Figure 6.3. This minor shift is not to be unexpected as the simulated synovial fluid ages, and galvanic interaction occurs between the metal and the fluid. However, above 100 Hz there is no significant deviation from the baseline data collected at the start of the test. Reviewing the electrochemical behavior of Samples D and E against Sample B and the test initiation data indicates significant deviation from the control and baseline above ~10 Hz. Samples D and E showed significantly lower magnitude of total impedance at high frequency, Figure 6.2. Total impedance magnitude of Sample D was nearly ½ of an order of magnitude smaller than the control sample, indicating significant potential for high frequency electrochemical reactions. Although Sample E closely followed the changes seen in Sample D, but to a lesser extent at high frequencies, the low frequency behavior of Sample E was markedly different from any other trend. Sample E showed the greatest amount of reactance, Figure 6.1, at low frequency, potentially indicating the possibility of increased capacitance like behavior. Each signal therefore elicits a separate, complex electrochemical behavior. This is the first documentation of this phenomenon within a simulated hip environment to the knowledge of the author, and requires significant study to develop a complete description and predication of the electrochemical response resulting from varying electrical signals on an implanted metal.

4. Discussion and interpretation

The electrical oscillation induced at the implant's surface, as represented by Sample D and E, incites active electrochemical reactions within the surrounding synovial fluid, generating surface modification through ion exchange and deposition growth. The type of surface modification is classified as direct corrosive/dissolution of the base material and as deposition growth, resulting in the development of wear particles. The distinction is pictorially described in the high magnification SEM images of Sample E given in Figure 7 below.

The direct corrosion/dissolution shown on the left of Figure 7 is categorized by the formation of pits on the metal's surface. This indicates that the metal has begun to directly dissolve into the synovial solution, causing direct degradation to the implant. This is in contrast to the deposition growth surface modification, shown on the right of Figure 7, in which solids precipitate out of solution and bond to the surface of the metal. The crystalline structure of the surface growth are then scraped from the implant's surface when subjected to mechanical wear during natural patient movement. The free crystalline structure then becomes imbedded within the surrounding tissue causing inflammation, pain, and leading to potential tissue necrosis. The corrosion then proceeds in a cyclic pattern until the implant must be revised or removed and replaced.

Additionally, the EIS characterization indicates the potential for increased electrochemical activity as the metal ages within the implanted environment. The decrease in the total magnitude of impedance at high frequency indicates the potential for a self-accelerating corrosive mode. It is therefore expected that this phenomenon may cause the unexpected rapid corrosion of hip implants after years of seemingly stable operation within the patient [18, 19, 20, 21].

This discovery rejects the traditional approach to metal corrosion within human subjects. Electrochemical surface reactions are active prior

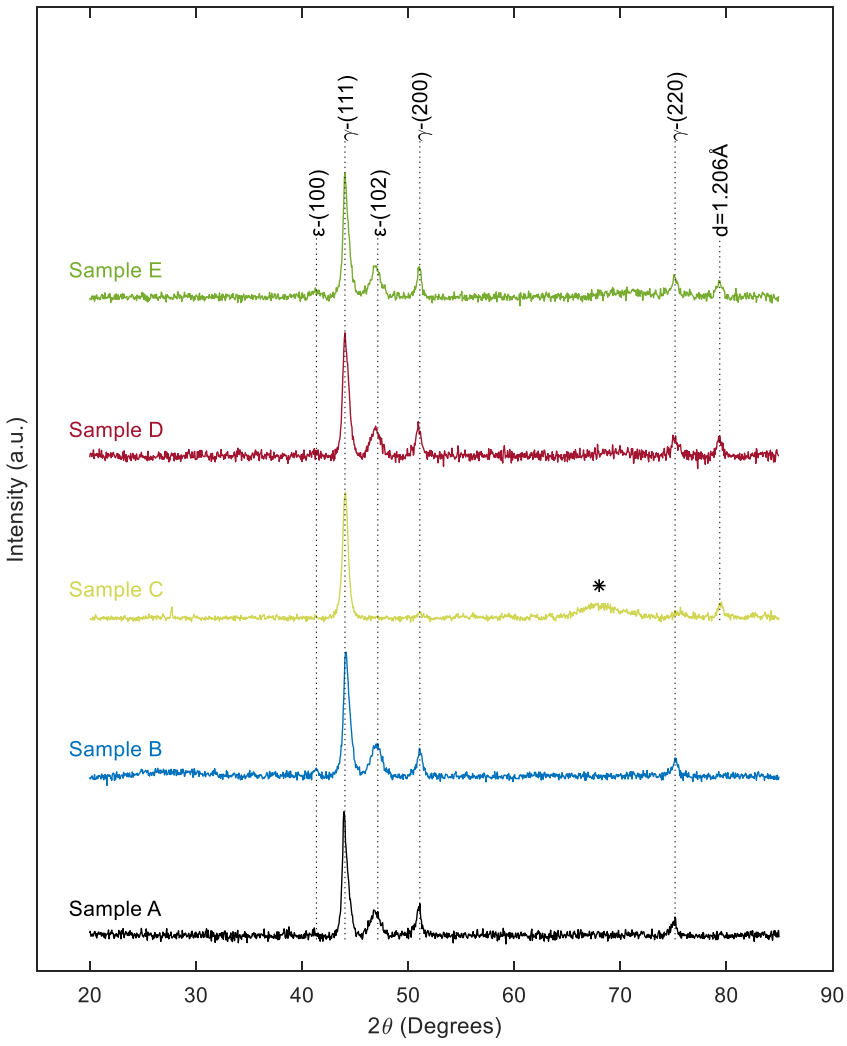

Figure 5. XRD patterns of base alloy and corrosion samples. Sample A: Baseline ASTM F75 CoCrMo alloy. Sample B: ASTM F75 CoCrMo alloy placed in simulated synovial fluid (50/50 DI water/FBS) with no electrical signal. Sample C: ASTM F75 CoCrMo alloy in simulated synovial fluid with $V_{rms} = 0.67$ V pulsed DC electrical signal. Sample D: ASTM F75 CoCrMo Alloy in simulated synovial fluid with 100 MHz Sine wave at 250 mV peak-to-peak amplitude AC electrical signal. Sample E: ASTM F75 CoCrMo alloy in simulated synovial fluid with 250 mV peak-to-peak amplitude random noise AC electrical signal.

to mechanical wear mechanisms, indicating that the electrochemical activity on the implant is a primary cause of breakdown and not a secondary or tertiary result of prior wear. Therefore, this electrochemical corrosion works in cooperation with fretting/crevice type corrosion for the complete breakdown of the implanted hip.

The exact electrical signal capable of replicating the complete chemical corrosion of implanted CoCrMo hip prosthetics must continue to be actively investigated. The work described here is the first viability study into the potential for natural electrical oscillations, developing on the prosthetic, to act as an incipient mechanism of corrosion. Significant further study is required to fully understand this phenomenon and its interdependencies on previously investigated fretting/crevice corrosion.

5. Broader relevance

Although CoCrMo ASTM F75 corrosion has been the focus of corrosion within the orthopedic industry, this phenomenon is expected to potentially be present in any implant containing metal. This particular corrosion was identified through hip replacement implants because of the immense number of hip replacement surgeries per year (~300,000/yr), and the reported patient pain in the surrounding tissue as the hip degrades [1, 2]. However, the increasing commonality of joint replacement surgeries, medical implants, and implantable biosensors combined with an increase in ambient electromagnetic activity of a technologically advanced society could result in significant unknown, adverse human health effects as metals corrode unexpectedly in the body [44].

Modern developments in biosensing have allowed for increased implementation of precision medicine practices [45, 46]. Precision medicine uses precise, directed action to treat and prevent patient morbidities with minimal medication and invasion beyond the target area, and is the underlying goal of many modern and future treatment methods. However, such targeted action requires significant knowledge and data for the particular morbidity and effected tissue. One of the most notable and common implementations of precision medicine, currently, is in the treatment of diabetes [47, 48, 49, 50]. Continuously monitoring glucose systems provide real time data of blood glucose levels for actionable response of insulin injection. Predictive algorithms can anticipate glucose level peaks and troughs for the individual user, decreasing the required amount of total medication used. These systems rely on an implanted biosensor that can simultaneously sense glucose level and transmit the data to a handheld receiver [49]. The transmitter is typically a metal based electrode manufactured from similar biocompatible alloys, as those within joint replacements mentioned previously [3, 46]. These sensors are typically changed every 30–90 days because of a thickened cell encapsulation layer of fibroblasts, fibrocytes, and collagen cells formed by the body's immunologic

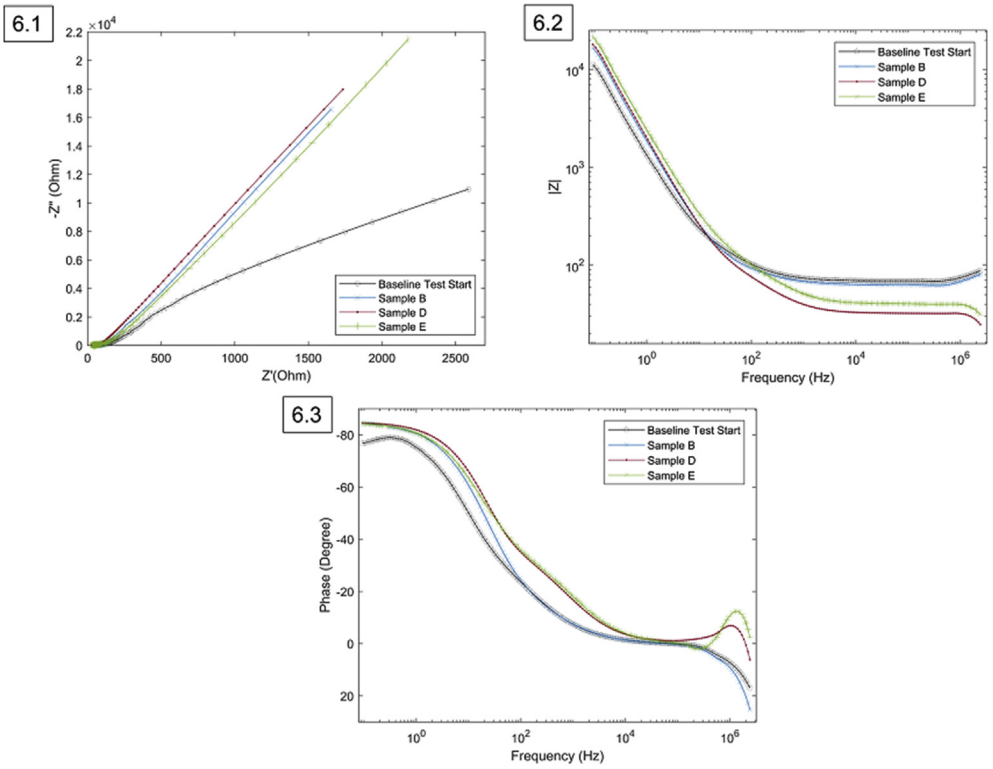

Figure 6. Micrographs of EIS analysis after 10 days of testing within the simulated synovial fluid test bed compared to the baseline scan on the first day of testing. Sample B: ASTM F75 CoCrMo alloy placed in simulated synovial fluid (50/50 DI water/FBS) with no electrical signal. Sample D: ASTM F75 CoCrMo Alloy in simulated synovial fluid with 100 MHz Sine wave at 250 mV peak-to-peak amplitude AC electrical signal. Sample E: ASTM F75 CoCrMo alloy in simulated synovial fluid with 250 mV peak-to-peak amplitude random noise AC electrical signal.

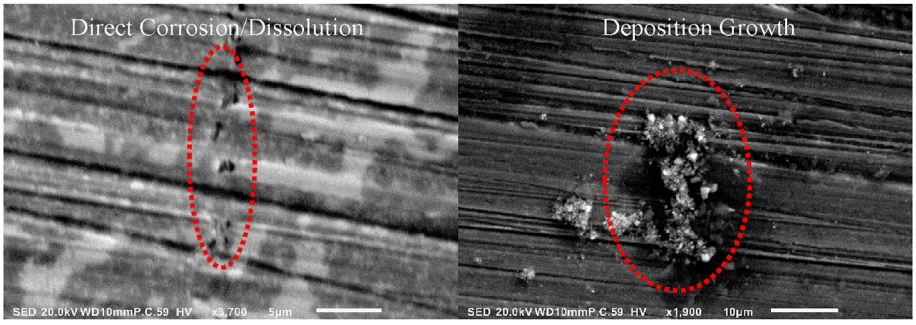

Figure 7. Comparison of surface modification types on Sample E under high magnification SEM imaging. Left: Direct corrosion/dissolution. Right: Deposition growth.

responses around the sensing probe that hinders accuracy [48]. The potential corrosion of these electrodes is not discussed because of the short implanted life and lack of mechanical wear on the sensor. However, this work indicates that the presence of electrical activity generated by the sensor itself could result in significant electrode corrosion and dissolution of metal into the body during the implanted life. Continual replacement and increased use of biosensors could lead to increased concern of metal toxicity within patients. The active electrochemical corrosion presented here could be considered in the future design of implanted devices and sensors.

Declarations

Author contribution statement

Thomas S. Welles: Conceived and designed the experiments; Performed the experiments; Analyzed and interpreted the data; Contributed reagents, materials, analysis tools or data; Wrote the paper.

Jeongmin Ahn: Conceived and designed the experiments; Analyzed and interpreted the data; Contributed reagents, materials, analysis tools or data; Wrote the paper.

Funding statement

This material is based upon work supported by the National Science Foundation (NSF) Graduate Research Fellowship Program (GRFP) under Grant No. 2019265542. Any opinions, findings, and conclusions or recommendations expressed in this material are those of the author(s) and do not necessarily reflect the views of the NSF.

Data availability statement

Data will be made available on request.

Declaration of interests statement

The authors declare no conflict of interest.

Additional information

No additional information is available for this paper.

References

[1] Total hip replacement - OrthoInfo - AAOS. https://orthoinfo.aaos.org/en/treatment/total-hip-replacement/. (Accessed 31 March 2020).

[2] Metal-on-Metal hip implant risks, Arthritis Foundation, https://www.arthritis.org/health-wellness/treatment/joint-surgery/safety-and-risks/metal-on-metal-hip-implant-risks. (Accessed 31 March 2020).

[3] C.Y. Hu, T.-R. Yoon, Recent updates for biomaterials used in total hip arthroplasty, Biomater. Res. 22 (2018) 33.

[4] S.-H. Park, Z. Lu, R.S. Hastings, et al., Five hundred fifty-five retrieved metal-on-metal hip replacements of a single design show a wide range of wear, surface features, and histopathologic reactions, Clin. Orthop. Relat. Res. 476 (2) (2018) 261–278.

[5] J.T. Munro, B.A. Masri, C.P. Duncan, D.S. Garbuz, High complication rate after revision of large-head metal-on-metal total hip arthroplasty, Clin. Orthop. Relat. Res. 472 (2) (2013) 523–528.

[6] J. Fritzsche, C. Borisch, C. Schaefer, Case report: high chromium and Cobalt levels in a pregnant patient with bilateral metal-on-metal hip arthroplasties, Clin. Orthop. Relat. Res. 470 (8) (2012) 2325–2331.

[7] J. Fritzsche, C. Borisch, C. Schaefer, Erratum to: case report: high chromium and Cobalt levels in a pregnant patient with bilateral metal-on-metal hip arthroplasties, Clin. Orthop. Relat. Res. 470 (9) (2012), 2626-2626.

[8] A.V. Lombardi, K.R. Berend, J.B. Adams, K.L. Satterwhite, Adverse reactions to metal on metal are not exclusive to large heads in total hip arthroplasty, Clin. Orthop. Relat. Res. 474 (2) (2016) 432–440.

[9] E. Gomez-Barrena, CORR Insights®: revision of metal-on-metal hip prostheses results in marked reduction of blood Cobalt and chromium ion concentrations, Clin. Orthop. Relat. Res. 473 (7) (2015) 2314–2315.

[10] J. Cawley, J. Metcalf, A. Jones, T. Band, D. Skupien, A tribological study of Cobalt chromium Molybdenum alloys used in metal-on-metal resurfacing hip arthroplasty, Wear 255 (7-12) (2003) 999–1006.

[11] K.R. Bridges, Iron absorption. http://sickle.bwh.harvard.edu/iron_absorption.html. (Accessed 29 April 2020).

[12] T. Ems, Biochemistry, Iron absorption. StatPearls [Internet], https://www.ncbi.nlm.nih.gov/books/NBK448204/. (Accessed 6 April 2020). Accessed April 29, 2020.

[13] V. Swaminathan, J.L. Gilbert, Fretting corrosion of CoCrMo and Ti6Al4V interfaces, Biomaterials 33 (22) (2012) 5487–5503.

[14] D. Royhman, M. Patel, J.J. Jacobs, et al., In vitro simulation of fretting-corrosion in hip implant modular junctions: the influence of pH, Med. Eng. Phys. 52 (2018) 1–9.

[15] R. Pourzal, D.J. Hall, J. Ehrich, et al., Alloy microstructure dictates corrosion modes in THA modular junctions, Clin. Orthop. Relat. Res. 475 (12) (2017) 3026–3043.

[16] H.S. Hothi, A.C. Panagiotopoulos, R.K. Whittaker, et al., Damage patterns at the head-stem taper junction helps understand the mechanisms of material loss, J. Arthroplasty 32 (1) (2017) 291–295.

[17] C.T. Penrose, T.M. Seyler, S.S. Wellman, et al., Complications are not increased with acetabular revision of metal-on-metal total hip arthroplasty, Clin. Orthop. Relat. Res. 474 (10) (2016) 2134–2142.

[18] S.A. Jones, CORR Insights®: complications are not increased with acetabular revision of metal-on-metal total hip arthroplasty, Clin. Orthop. Relat. Res. 474 (10) (2016) 2143–2144.

[19] A. Di Laura, P.D. Quinn, V.C. Panagiotopoulou, et al., The chemical form of metal species released from corroded taper junctions of hip implants: synchrotron analysis of patient tissue, Sci. Rep. 7 (1) (2017).

[20] F. Eltit, Q. Wang, R. Wang, Mechanisms of adverse local tissue reactions to hip implants, Front. Bioeng. Biotechnol. 7 (JUL) (2019).

[21] R.H. Oskouei, M.R. Barati, H. Farhoudi, et al., New finding on the in-vivo crevice corrosion damage in a CoCrMo hip implant, Mater. Sci. Eng. C 79 (2017) 390–398.

[22] N.R. Glaviano, S. Huntsman, A. Dembeck, et al., Improvements in kinematics, muscle activity and pain during functional tasks in females with patellofemoral pain following a single patterned electrical stimulation treatment, Clin. Biomech. 32 (2016) 20–27.

[23] K. Sykes, Y.M. Wong, Electrical activity of vastus medialis oblique muscle in straight leg raise exercise with different angles of hip rotation, Physiotherapy 89 (7) (2003) 423–430.

[24] C. Ionescu-Tirgoviste, P.A. Gagniuc, E. Gagniuc, The electrical activity map of the human skin indicates strong differences between normal and diabetic individuals: a gateway to onset prevention, Biosens. Bioelectron. 120 (2018) 188–194.

[25] R. Zhang, M. Hummelgård, J. Örtegren, et al., Sensing body motions based on charges generated on the body, Nano Energy 63 (2019) 103842.

[26] J.R. Gray, C.H. Frith, J.D. Parker, In vivo enhancement of chemotherapy with static electric or magnetic fields, Bioelectromagnetics 21 (2000) 575–583.

[27] K.R. Skulberg, K. Skyberg, W. Eduard, et al., Effects of electric field reduction in visual display units on skin symptoms, Scand. J. Work. Environ. Health 27 (2001) 140–145.

[28] G. Oftedal, A.I. Vistnes, K. Rygge, Skin symptoms after the reduction of electric fields from visual display units, Scand. J. Work. Environ. Health 21 (1995) 335–344.

[29] J.P. Blondin, D. Nguyen, J. Sheghen, et al., Human perception of electric fields and ion currents associated with high-voltage DC transmission lines, Bioelectromagnetics 17 (1996) 230–241.

[30] T.W. Dawson, M.A. Stuchly, R. Kavet, Electric fields in the human body due to electrostatic discharges, IEEE Trans. Biomed. Eng. 51 (2004) 1460–1468.

[31] S. Lagorio, M. Röösli, Mobile phone use and risk of intracranial tumors: a consistency analysis, Bioelectromagnetics 35 (2014) 79–90.

[32] H. Odagiri-Shimizu, K. Shimizu, Experimental analysis of the human perception threshold of a DC electric field, Med. Biol. Eng. Comput. 37 (1999) 727–732.

[33] G. Ziegelberger, P. Vecchia, M. Hietanen, et al., Guidelines on limits of exposure to static magnetic fields, Health Phys. 9 (2009) 504–514.

[34] C.J. Pan, L. Subramanyam, B.J. Hwang, Formation and characterization of bimetallic nanoparticles in electrochemistry, in: Handbook of Nanoelectrochemistry: Electrochemical Synthesis Methods, Properties, and Characterization Techniques, 2016, pp. 169–240.

[35] J.R. Lott, H.B. McCain, Some effects of continuous and pulsating electric fields on brain wave activity in rats, Int. J. Biometeorol. 17 (1973) 221–225.

[36] W.T. Kaune, Power-frequency electric fields averaged over the body surfaces of grounded humans and animals, Bioelectromagnetics 2 (1982) 403–406.

[37] Y. Xu, S. Wu, G. Di, et al., Influence of static electric field on cognition in mice, Bioengineered 7 (2016) 241–245.

[38] G. Sahakyan, H. Harutyunyan, G. Artsruni, Biological activity of external electrostatic field exceeding the natural background: erythrocyte plasma membrane target, Int. J. Sci. Res. Environ. Sci. 3 (2015) 88–98.

[39] Z. Xia, B.F. Ricciardi, Z. Liu, et al., Nano-analyses of wear particles from metal-on-metal and non-metal-on-metal dual modular neck hip arthroplasty, Nanomed. Nanotechnol. Biol. Med. 13 (3) (2017) 1205–1217.

[40] Z. Guo, X. Pang, Y. Yan, et al., CoCrMo alloy for orthopedic implant application enhanced corrosion and tribocorrosion properties by nitrogen ion implantation, Appl. Surf. Sci. 347 (2015) 23–34.

[41] S.H. Lee, E. Takahashi, N. Nomura, A. Chiba, Effect of carbon addition on microstructure and mechanical properties of a wrought Co–Cr–Mo implant alloy, Mater. Trans. 47 (2006) 287–290.

[42] C. Liu, Z. Zhou, K.Y. Li, Improved corrosion resistance of CoCrMo alloy with self-passivation ability facilitated by carbon ion implantation, Electrochim. Acta 241 (2017) 331–340.

[43] W. Zai, M. Wong, H. Man, Improving the wear and corrosion resistance of CoCrMo-UHMWPE articulating surfaces in the presence of an electrolyte, Appl. Surf. Sci. 464 (2019) 404–411.

[44] T. Stieglitz, M. Schuettler, Material-tissue interfaces in implantable systems, in: Implantable Sensor Systems for Medical Applications, Elsevier Ltd., 2013, pp. 39–67.

[45] J.X.J. Zhang, K. Hoshino, Implantable sensors, in: Molecular Sensors and Nanodevices, Elsevier, 2014, pp. 415–465.

[46] S. Martin, E. Duncan, Sterilisation considerations for implantable sensor systems, in: Implantable Sensor Systems for Medical Applications, Elsevier Ltd., 2013, pp. 253–278.

[47] J. Kropff, P. Choudhary, S. Neupane, et al., Accuracy and longevity of an implantable continuous glucose sensor in the precise study: a 180-day, prospective, multicenter, pivotal trial, Diabetes Care 40 (1) (2017) 63–68.

[48] Continuous glucose monitoring sensor | eversense CGM. https://www.eversensediabetes.com/sensor. (Accessed 31 March 2020).

[49] L. Tang, K. Huan, D. Deng, et al., Glucose sensor based on Pd nanosheets deposited on Cu/Cu2O nanocomposites by galvanic replacement, Colloids Surf. B Biointerfaces 188 (2020) 110797.

[50] Y. Dilmac, M. Guler, Fabrication of non-enzymatic glucose sensor dependent upon Au nanoparticles deposited on carboxylated graphene oxide, J. Electroanal. Chem. 864 (2020) 114091.